

Modeling of Cdc25B Dual Specificity Protein Phosphatase Inhibitors: Docking of Ligands and Enzymatic Inhibition Mechanism

Antonio Lavecchia,* Sandro Cosconati, Vittorio Limongelli, and Ettore Novellino^[a]

The Cdc25 dual specificity phosphatases have central roles in coordinating cellular signalling processes and cell proliferation. It has been reported that an improper amplification or activation of these enzymes is a distinctive feature of a number of human cancers, including breast cancers. Thus, the inhibition of Cdc25 phosphatases might provide a novel approach for the discovery of new and selective antitumor agents. By using the crystal structure of the catalytic domain of Cdc25B, structural models for the interaction of various Cdc25B inhibitors (1–13) with the enzyme were generated by computational docking. The parallel use of two efficient and predictive docking programs, AutoDock and GOLD, allowed mutual validation of the predicted binding poses. To evaluate their quality, the models were validated with known

structure–activity relationships and site-directed mutagenesis data. The results provide an improved basis for structure-based ligand design and suggest a possible explanation for the inhibition mechanism of the examined Cdc25B ligands. We suggest that the recurring motif of a tight interaction between the inhibitor and the two arginine residues, 482 and 544, is of prime importance for reversible enzyme inhibition. In contrast, the irreversible inhibition mechanism of 1–4 seems to be associated with the close vicinity of the quinone ring and the Cys473 catalytic thiolate. We believe that this extensive study might provide useful hints to guide the development of new potent Cdc25B inhibitors as novel anticancer drugs.

Introduction

Tyrosine phosphorylation of proteins is a fundamental mechanism of intracellular signal transduction and is involved in important cellular events such as cell growth and differentiation.^[1] The phosphorylation states of proteins are strictly controlled by various protein tyrosine kinases (PTKs) and protein tyrosine phosphatases (PTPs). PTKs catalyze the covalent attachment of phosphate groups to the amino acid side chain of proteins, whereas PTPs catalyze the removal of this group. Eukaryotic protein phosphatases can be divided into two main subclasses^[2–4] based upon their substrate specificity and protein structure: protein serine/threonine phosphatases (PSTPs), which dephosphorylate phosphoserine (pSer) and phosphothreonine (pThr) in a single-step reaction by using a metal-activated water molecule, and protein tyrosine phosphatases (PTPs) which dephosphorylate phosphotyrosine (pTyr) in a two-step reaction involving a cysteinyl-phosphate enzyme intermediate. Dual-specificity protein phosphatases (DSPs), which dephosphorylate both pTyr and pThr residues, are considered to be a subfamily of PTPase because they possess the conserved PTPs signature motif HCX₅R, and they employ a similar catalytic mechanism.^[5,6] Cdc25 cell-cycle regulators are examples of DSPs that dephosphorylate contiguous pTyr and pThr on cyclin-dependent kinases (CdKs), and have been shown to play crucial roles in cell proliferation.^[7]

Three Cdc25 homologues, Cdc25A, Cdc25B, and Cdc25C, are encoded by the human genome. Cdc25A and B have oncogen-

ic properties.^[8] They are transcriptional targets of the c-Myc oncogene^[9] and are overexpressed in many human tumors.^[8,10] Both Cdc25B and Cdc25C are thought to be regulators of the G₂–M transition through their ability to dephosphorylate and activate the Cdk1–cyclinB mitotic kinase complex, which is required for cell entry into mitosis.^[7] Cdc25A is likely to be important for the G₁–S phase transition and in preserving genomic integrity,^[11] although Cdc25A might also have some role in the initiation of mitosis.^[12] Cdc25A is rapidly degraded in response to DNA damage, which impairs the G₁–S transition.^[13]

Due to their functional role, Cdc25s have been studied extensively. Broad evidence suggests that improper amplification or activation of Cdc25A or Cdc25B is a distinctive feature of a number of human cancers, including breast cancers.^[14] Moreover, augmented expression of Cdc25A or B results in cellular transformation, and the transcription and catalytic activities of both proteins are directly regulated by two other protooncogene products, c-Myc and c-Raf, respectively.^[8,9,15] Thus, deregulation of Cdc25A and Cdc25B activities, either through over-

[a] Prof. Dr. A. Lavecchia, Dr. S. Cosconati, Dr. V. Limongelli, Prof. Dr. E. Novellino
Dipartimento di Chimica Farmaceutica e Tossicologica
Università di Napoli "Federico II"
Via D. Montesano, 49, 80131 Napoli (Italy)
Fax: (+39) 081-678-613
E-mail: lavecchi@unina.it

expression or abnormal activation, might contribute to the growth of certain types of cancer. Therefore, due to their reported oncogenic properties, Cdc25 inhibition could represent a new and valuable approach in cancer therapy.^[16]

Although the crystal structures of the catalytic domains of Cdc25A and Cdc25B have been reported at 2.3 Å^[17] and 1.9 Å resolution,^[18] respectively, a detailed description of their interactions with small-molecule inhibitors has never been reported. A comparison of the two crystal structures revealed similarity within the catalytic domain. As expected, both phosphatases contain the canonical HCX₅R PTPase catalytic-site motif, in which H is a highly conserved histidine residue, C is the catalytic cysteine, Xs are the five residues that form a loop in which all of the amide nitrogens hydrogen bond to the phosphate of the substrate, and R is a highly conserved arginine that hydrogen bonds to the phosphorylated amino acid of the substrate. However, key differences in the positions of residues believed to be essential for catalysis between Cdc25A and Cdc25B, were observed. For example, the carbonyl group of residue 434 in Cdc25A (residue 477 in Cdc25B) points toward the location where phosphate should bind; the opposite of that observed with Cdc25B and other PTPs.^[19] A difference in the positioning of the side chain for Arg436 in Cdc25A was also observed, which appears to be misplaced when compared to the structures of the Cdc25B catalytic domain and other known phosphatases. In fact, the corresponding Arg479 in Cdc25B, forms a hydrogen bond with Glu431, which is comparable to that observed with other PTPs. Cdc25A failed to bind oxyanions in its catalytic site, whereas Cdc25B readily bound tungstate and sulfate in a mode similar to other PTPases and DSPases.^[18] The Cdc25A catalytic domain also lacks any loops proximal to the active site that could facilitate substrate binding.^[17,18] Finally, another major difference between the Cdc25B catalytic domain structure and the Cdc25A structure is in the C-terminal region (residues 531–547, Cdc25B numbering). This region of Cdc25B, which is well resolved in the crystal structure, contains an α -helix that is positioned against the bulk of the protein. Several residues of the helix, such as Met531 and Arg544, point toward the active-site cleft. In contrast to the Cdc25A structure, this region is undefined beyond Asp492 (Cdc25A numbering scheme), and the few residues that are observed appear to be misplaced. For example, the sequence is directed away from the active site of the protein and toward a symmetrically related molecule in the crystal. This results in a more open structure,^[18] which is not suitable for the structure-based design of compounds with complementary binding surfaces.

For the above-mentioned reasons, no reliable information about ligand binding

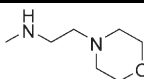
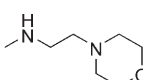
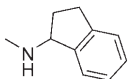
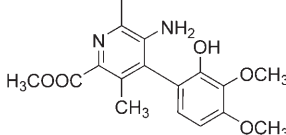
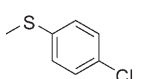
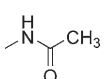
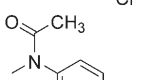
can be directly obtained from the Cdc25A protein structure. The highly resolved and more compacted crystal structure of the Cdc25B catalytic domain however, seems to be more suitable for rational inhibitor design.

This paper reports a molecular-docking analysis of selective reversible Cdc25B inhibitors by using the published crystal structure of the Cdc25B catalytic domain (PDB ID: 1QB0)^[18] in order to explore the ligand-binding mode and to clarify the molecular basis for the inhibitory activity of the selected compounds. All ligand–enzyme complexes were predicted by two automatic docking programs, namely AutoDock^[20,21] and GOLD,^[22–24] which have been shown to be highly effective at reproducing experimentally found binding modes of other ligands.^[20,21,24] Moreover, the resulting docking poses were scored and ranked by using the native scoring function implemented in the respective docking programs.

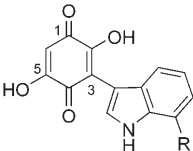
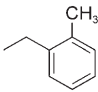
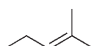
For docking experiments, we chose a highly diverse set of synthetic competitive Cdc25B inhibitors with inhibitory potencies ranging from micromolar to nanomolar values. The structures of the investigated ligands are shown in Tables 1–4.

A set of inhibitory compounds was identified from an in vitro screening of the NCI's chemical substances against oncogenic, full-length, recombinant human Cdc25B.^[25] Twenty-one compounds were found to have a mean inhibitory concentration of less than 1 μ M. Among these, we decided to investigate the most structurally representative inhibitors 1–4, which had IC₅₀ values of 0.30 μ M, 0.21 μ M, 0.82 μ M, and 0.37 μ M, respectively. In the same study, Lazo et al. also found the potent naphthoquinones 5 (IC₅₀ = 0.62 μ M) and 6 (IC₅₀ = 0.85 μ M; Table 1).

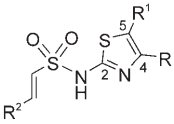
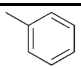
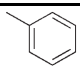
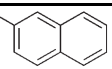
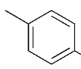
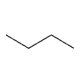
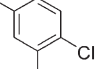
Table 1. Reported IC₅₀ values for quinolinequinones 1–4 and naphthoquinones 5 and 6.

Compd	R	R ¹	R ²	IC ₅₀ [μ M]	Ref.
1	Cl		H	0.21 ± 0.08	[25]
2		Cl	H	0.82 ± 0.08	[25]
3	Cl		H	0.30 ± 0.03	[25]
4	OCH ₃	NH ₂		0.37 ± 0.08	[25]
5			H	0.62 ± 0.10	[25]
6		H	H	0.89 ± 0.09	[25]

Later on, Sohn et al.^[26] described an indolyldihydroxyquinone class of reversible Cdc25B inhibitors that bind to the active site with submicromolar potency. Structure–activity relationship (SAR) studies led to the discovery of 50 derivatives. We focused on compounds **7** and **8**, which were the most potent and had IC₅₀ values of 1.0 μM and 5.6 μM, respectively (Table 2).

Table 2. Reported IC ₅₀ values for indolyldihydroxyquinones 7 and 8 .				
				
Compd	R	IC ₅₀ [μM]	Ref.	
7		1.00 ± 0.20	[26]	
8		5.60 ± 1.12	[26]	

A library of sulfonylated aminothiazoles was also prepared and screened for inhibitory activity against Cdc25B, VHR, and PTP1B.^[27] From the best inhibitors, we chose compounds **9** and **10** (Table 3), which had IC₅₀ values of 22 μM and 21 μM, respectively.

Table 3. Reported IC ₅₀ values for sulfonylated aminothiazoles 9 and 10 .					
					
Compd	R	R ¹	R ²	IC ₅₀ [μM]	Ref.
9				22 ± 2.00	[27]
10				21 ± 4.00	[27]

Finally, docking simulations were undertaken on structurally dissimilar compounds **11–13**,^[28–30] which were reported to inhibit Cdc25B phosphatase with IC₅₀ values of 11 μM, 3.9 μM and 0.17 μM, respectively (Table 4).

Results

The compounds shown in Tables 1–4 revealed a consistent set of recurring binding modes. For all investigated compounds, AutoDock provided well-clustered docking results. As shown in Table 5, the 50 independent docking runs carried out for each ligand generally converged to a small number of different po-

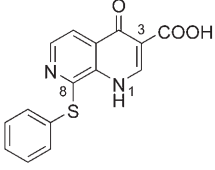
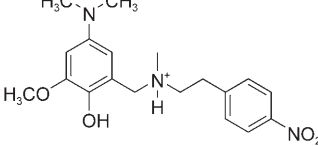
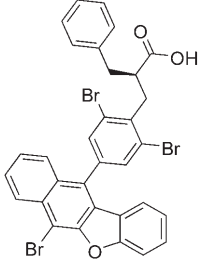
Table 4. Reported IC ₅₀ values for diverse Cdc25B inhibitors 11–13 .			
Compd	Structures	IC ₅₀ [μM]	Ref
11		5.00	[28]
12		3.90 ± 0.01	[29]
13		0.17 ± 0.10	[30]

Table 5. Results of 50 independent AutoDock and GOLD docking runs for each ligand. ^[a]				
Ligand	N _{tot}	f _{occ}	ΔG _{bind}	GOLD score ^[b]
1	10	26	−8.12	42.97
2	14	23	−8.48	32.48
3	16	14	−8.63	35.27
4	16	20	−7.86	49.72
5	11	11	−7.89	52.28
6	13	10	−8.29	50.38
7	6	20	−9.16	51.36
7	6	7	−8.64	
8	8	12	−8.06	44.46
8	8	8	−7.73	
9	12	19	−6.13	30.72
10	12	20	−6.15	31.82
11	18	8	−6.80	55.31
12	33	10	−7.70	32.61
13	15	19	−9.48	66.52

[a] N_{tot} is the total number of clusters; the number of results in the top cluster is given by the frequency of occurrence, f_{occ}. ΔG_{bind} is the estimated free energy of binding for the best cluster results and is given in kcal mol^{−1}. [b] Higher scores indicate more favorable binding.

sitions (“clusters” of results differing by less than 1.5 Å rmsd). Generally, the top ranking clusters (i.e., those with the most favorable free energy of binding ΔG_{bind}) occurred most frequently; this suggests good convergence behavior from the search algorithm. The best results in terms of free energy of binding were all located in a comparable position in the active site.

GOLD provided docking solutions in which the majority of ligands occupied the same binding location as suggested by AutoDock. The result from a GOLD run is a series of viable conformations of the ligand docked inside the binding site of the

target protein, together with an associated scoring function and other measures of the corresponding protein–ligand interaction energy. The GOLD score consists of hydrogen-bonding, complex energy, and ligand internal-energy terms. Since there is a large number of hydrogen donor–acceptor pairs within the Cdc25B active site, the GOLD score was expected to properly rank the ligand poses after the docking. Although both the estimated AutoDock free energies of binding and GOLD scores represent useful descriptors of ligand–receptor complementarity, the choice of the “best” docking model was also dictated by its agreement with the SARs and the site-directed mutagenesis data. Docking results are summarized in Table 5, and a graphical representation of the binding modes of the most structurally representative derivatives **1**, **4**, **5**, **7**, **9**, and **11–13** is given in Figures 1–9. For each inhibitor, the results are briefly described in the following section.

Quinolinequinones 1–4

A distinct binding pose was found for compounds **1–4** with highly populated clusters ($f_{\text{occ}}=26/50$, $23/50$, $14/50$, and $20/50$, respectively), and estimated binding free energies of -8.12 , -8.48 , -8.63 , and -7.86 kcal mol $^{-1}$, respectively (Table 5).

As depicted in Figure 1 a, compound **1** forms a network of hydrogen bonds and electrostatic interactions between the quinone carbonyl oxygens at positions 5 and 8, and the Arg544, Arg482, and Tyr428 side chains. Moreover, the nitrogen atom at position 1 of the same moiety accepts an additional hydrogen bond from Arg482. The morpholine oxygen atom is engaged in a hydrogen bond with both the Phe475 NH backbone and the Arg479 side chain.

AutoDocking of compound **2**, which is the regioisomer of **1**, resulted in a binding position featuring the quinolinequinone moiety in the same spatial location as **1**, although it appears to be in an inverted position. This pose not only allows the occurrence of electrostatic interactions between the quinone carbonyl oxygens and Arg482, Arg544, and Tyr428, but also orients the morpholinoethylamino chain toward the catalytic Phe475 NH backbone and Arg479, thus establishing the same sort of interactions as de-

scribed for **1**. This might explain the comparable IC $_{50}$ values found for compounds **1** and **2**.

A similar binding mode was also found for compound **3**, which occupies the same spatial position as **1** in the binding site and also establishes analogous hydrogen bonds and electrostatic interactions with the enzyme. This binding pose is further stabilized by the occurrence of a T-shaped interaction between the aromatic ring of the ligand–indanyl moiety and the catalytic Phe475 side-chain. For compound **4**, AutoDock calculated a top-ranking solution that showed a network of hydrogen bonds between the quinone carbonyl oxygens and both Arg482 and Arg544 side chains (Figure 2a). This binding pose is further stabilized by an additional hydrogen bond between the COOCH $_3$ ester oxygen and the Arg479 side chain.

Different binding modes of **1–4** were found when docking was performed with GOLD. This program predicted comparable solutions for compounds **1** and **2**. Interestingly, both of the top-scoring solutions (42.97 and 32.48 , respectively) placed the quinolinequinone ring into the catalytic site of Cdc25B differently from what was suggested by AutoDock (Figure 1 b). In particular, one quinone carbonyl oxygen, situated near the cat-

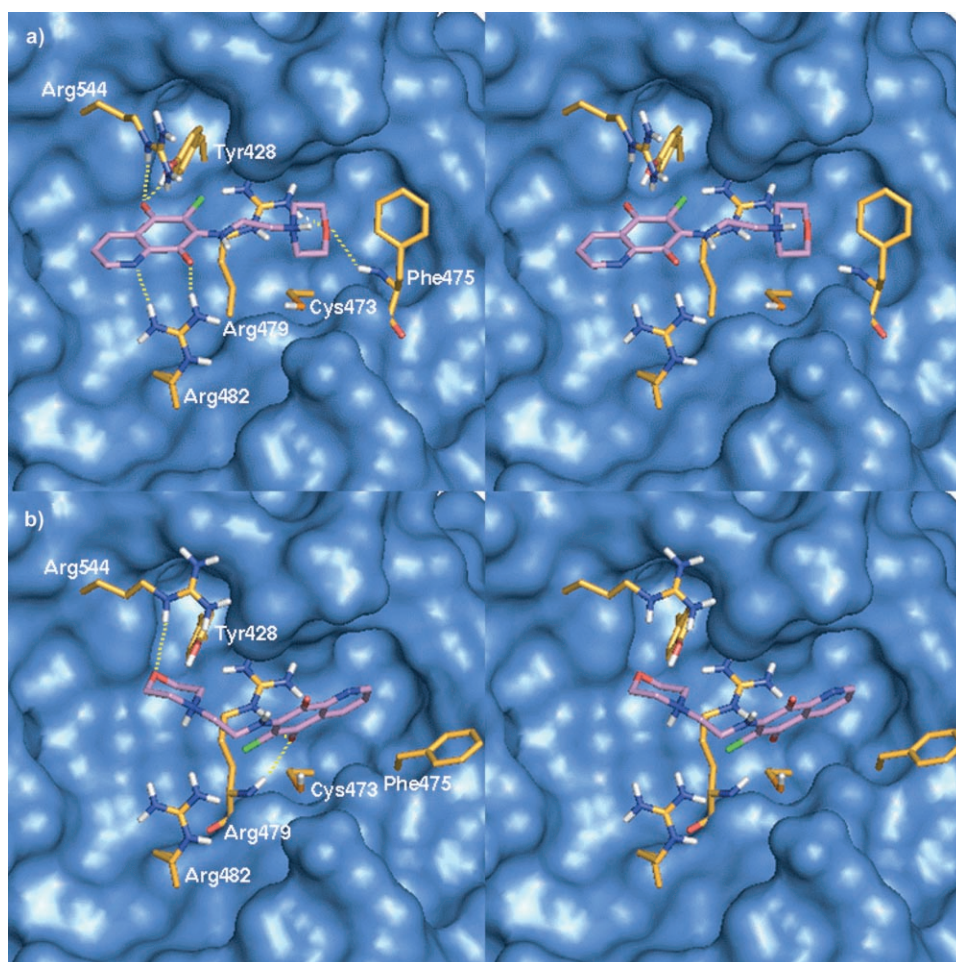


Figure 1. Stereoviews of the alternative binding modes of compound **1** in the Cdc25B binding cavity as calculated by a) Autodock and b) GOLD. For clarity, only interacting residues are displayed. The ligand (violet) and interacting key residues (orange) are represented as stick models, while the protein as a Connolly surface. H-bonds are shown as dashed yellow lines.

alytic Cys473, forms hydrogen bonds with both the Arg479 NH backbone and the side chain of the same residue, while the ligand's morpholine oxygen is involved in an additional hydrogen bond with Arg544. The only difference displayed by the calculated binding position for the regioisomer **2** resides in the inverted position of the quinoline-quinone ring. For compound **3**, GOLD predicted a top-scoring solution (35.27), and fit **3** into the enzyme's catalytic site similarly to what was found for **1**. Interestingly, when analyzing the other binding modes calculated by GOLD for compounds **1** and **2**, we found that the second and the third solutions were virtually identical to those found by AutoDock for these compounds. From this point of view, it could be inferred that two different binding modes are feasible for **1–3**, and the best one cannot be determined unambiguously.

GOLD was able to calculate a top-scoring solution for compound **4** (49.72), and it also placed the quinone ring in the same pocket as was found for **1–3**. As illustrated in Figure 2b, the quinone amino group donates a hydrogen bond to the Glu474 side chain, the pyridine nitrogen atom accepts two hydrogen bonds from the Tyr428 and Arg544 side chains, and the CO₂CH₃ carbonyl oxygen at position 6 of the same ring still forms an electrostatic interaction with Arg544. This binding mode is further stabilized by the occurrence of two hydrogen bonds between both the phenolic and methoxy oxygens of the pendant phenyl ring and the Arg482 side chain.

Naphthoquinones **5** and **6**

A well-clustered binding pose was found by AutoDock for naphthoquinones **5** ($f_{\text{occ}}=11/50$, $\Delta G_{\text{bind}}=-7.89$) and **6** ($f_{\text{occ}}=10/50$, $\Delta G_{\text{bind}}=-8.29$ kcal mol⁻¹), which featured the same recurring electrostatic interactions be-

tween the quinone carbonyl oxygens and the corresponding Arg544 and Arg482 side chains for both molecules (Figure 3). An additional hydrogen bond is observed between the qui-

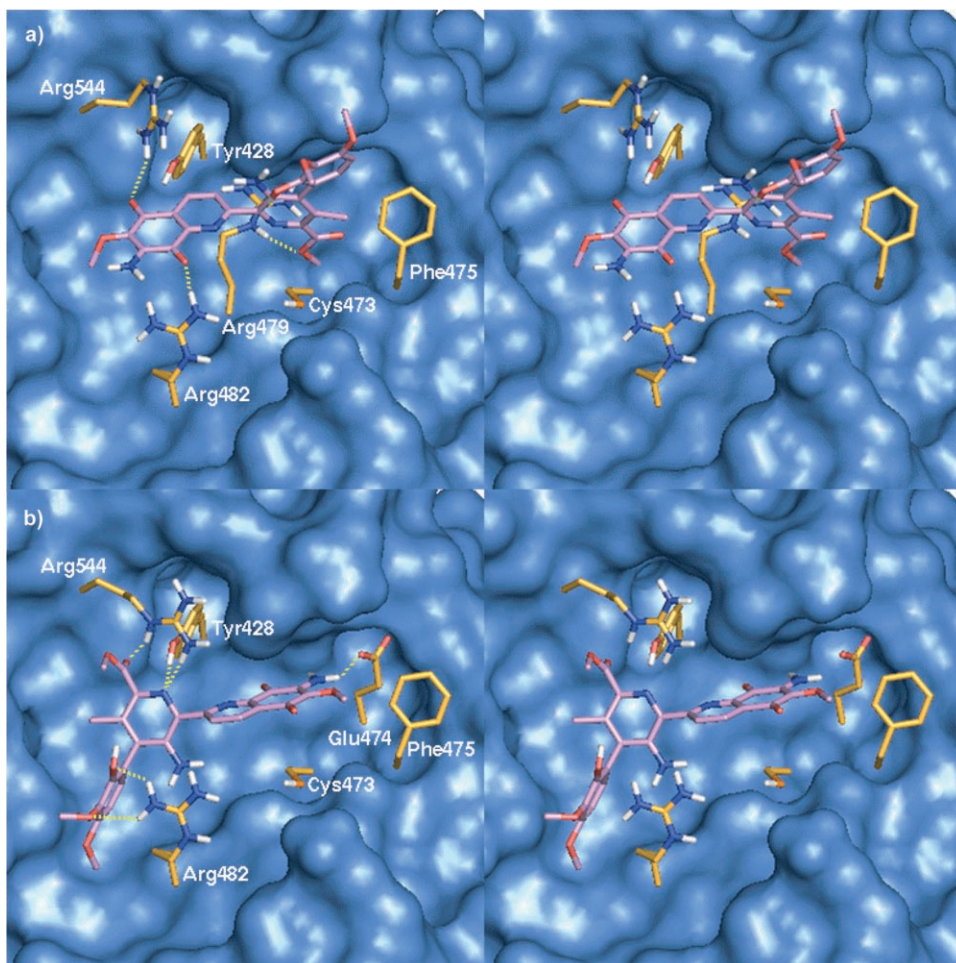


Figure 2. Stereoviews of the alternative binding modes of compound **4** in the Cdc25B binding cavity as calculated by a) Autodock and b) GOLD.

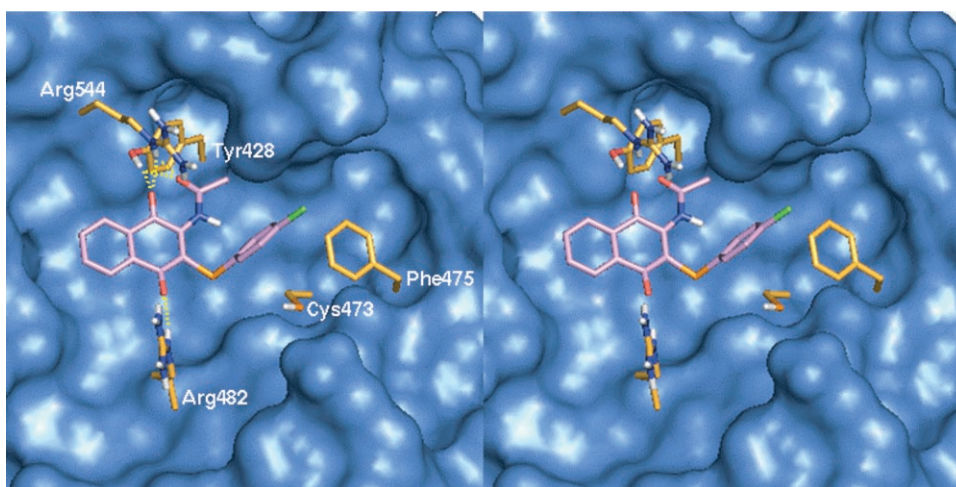


Figure 3. Stereoview of the binding mode of compound **5** in the Cdc25B binding cavity as calculated by both Autodock and GOLD.

none oxygen at position 4 and Tyr428. This residue together with Arg544 donates a hydrogen bond to the carbonyl oxygen of the acetamide group at position 2 of **5**, while the *p*-chlorophenylthio substituent at position 3 penetrates deeper into the catalytic binding site and establishes a T-shaped interaction with the Phe475 aromatic ring.

Surprisingly, GOLD was able to locate the same binding modes found by AutoDock for both compounds, **5** and **6**. This increased our confidence in the reliability of the predicted poses.

Indolyldihydroxyquinones **7** and **8**

The docking of **7** into the Cdc25b catalytic pocket provided well-clustered solutions; the top result had a much better score than all other results ($\Delta G_{\text{bind}} = -9.16 \text{ kcal mol}^{-1}$, found 20 times out of 50). Similarly, the top-ranked binding mode obtained for **8** ($\Delta G_{\text{bind}} = -8.06 \text{ kcal mol}^{-1}$, found 12 times out of 50) was located in a comparable position at the active site.

As shown in Figure 4a, the quinone carbonyl oxygen at position 4 of **7** and the hydroxy group at position 5 are involved in hydrogen bonds with the Arg482 and Thr547 side chains, re-

spectively. Similarly, the quinone carbonyl oxygen at position 1 also forms hydrogen bonds with Arg482. The 7-(2-methyl-benzyl)indolyl chain adapts itself into the Cdc25B catalytic site, establishing a T-shaped interaction with the Phe475 side chain. It is worth noting, that the indole moiety of **8**, together with its dimethylallyl chain, also fits into the catalytic site of Cdc25B, although the additional charge-transfer interaction with Phe475 is lost. This might explain the higher inhibitory activity of **7** compared to **8**.

A significant alternative to this position is given by the second cluster. Although it was found less frequently, it showed only a slight energy difference compared to the top result for compounds **7** and **8**. As shown in Figure 4b, this solution places the dihydroxyquinone ring in the Cdc25B catalytic site and the 7-(2-methyl-benzyl)indolyl chain between Arg482 and Arg544. The quinone carbonyl oxygen at position 4 is engaged in hydrogen bonds with the Arg479 NH backbone and the side chain of the same residue, while the hydroxy group at position 5 is within hydrogen-bonding distance of the catalytic backbone NHs of Phe475, Ser477, and Glu478.

In contrast to AutoDock, GOLD successfully calculated a single solution for compounds **7** and **8**. Surprisingly, the associated binding orientations strongly resembled the second-ranking ones found by AutoDock with scores of 51.36 for **7** and 44.46 for **8**. The convergence toward a single solution in GOLD might support the preference for this binding position rather than for the first-ranking one calculated by AutoDock.

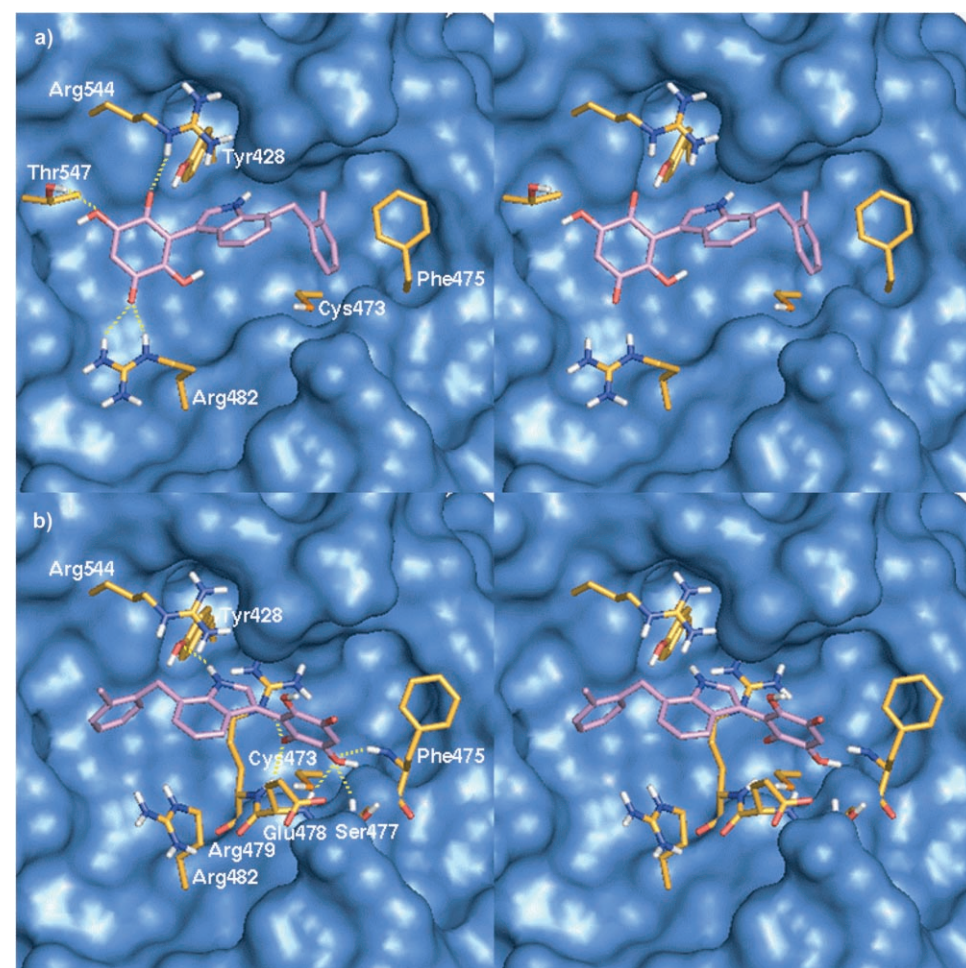


Figure 4. Stereoviews of the alternative binding modes of compound **7** in the Cdc25B binding cavity as calculated by a) Autodock and b) GOLD.

Sulfonylated aminothiazoles **9** and **10**

AutoDock calculations for compound **9** converged to a small number of clusters. The most populated one ($f_{\text{occ}} = 19/50$) had a ΔG_{bind} of $-6.13 \text{ kcal mol}^{-1}$. The ligand is found in the center of the Cdc25B active site (Figure 5).

One of the sulfonamide oxygens is involved in two hydrogen bonds with the Arg544 side chain, while the phenyl ring at position 4 points toward the catalytic site of the enzyme; this establishes a charge-transfer interaction with the Phe475 aromatic ring. A similar binding pose was predicted for compound **10** ($\Delta G_{\text{bind}} = -6.15 \text{ kcal mol}^{-1}$, found 20 times out of 50), which displayed polar interactions almost identical to those found for **9**.

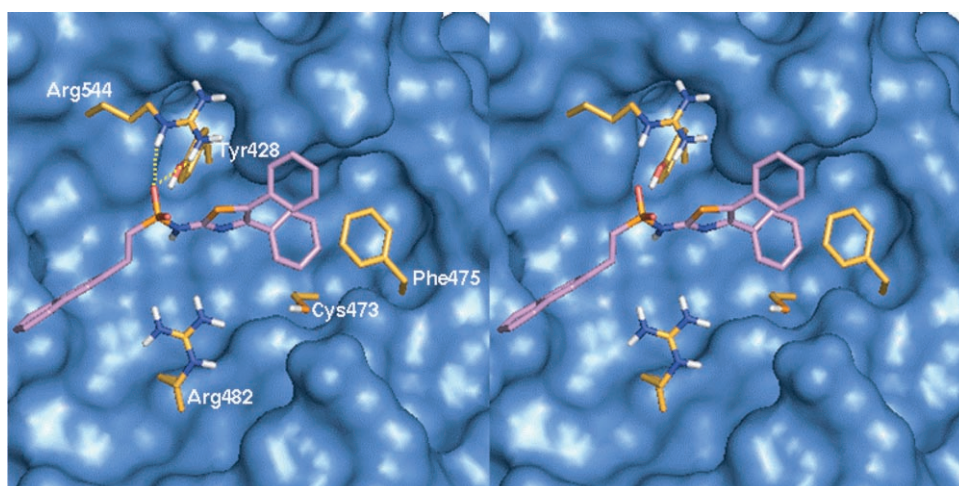


Figure 5. Stereoview of the binding mode of compound **9** in the Cdc25B binding cavity as calculated by both Autodock and GOLD.

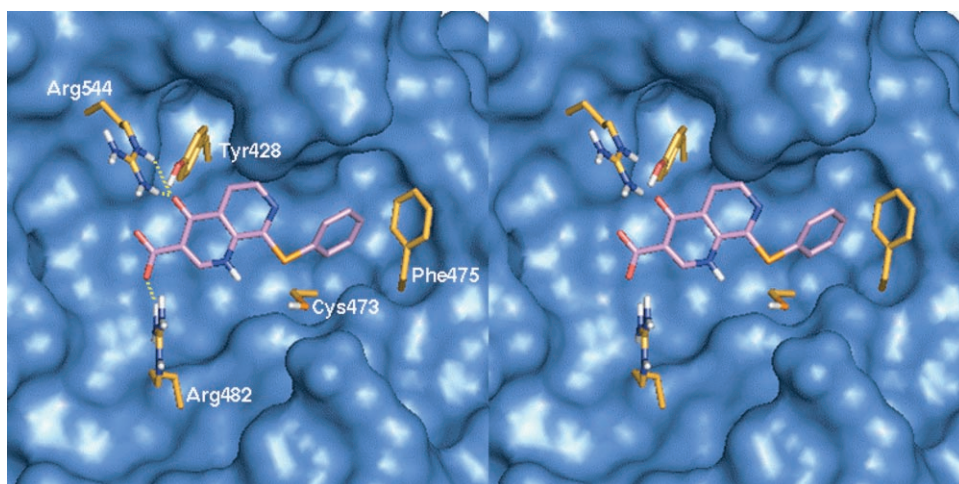


Figure 6. Stereoview of the binding mode of compound **11** in the Cdc25B binding cavity as calculated by both Autodock and GOLD.

The reported binding mode was also predicted by GOLD with a scores of 30.72 for **9** and 31.82 for **10**.

Compounds 11–13

Interestingly, both AutoDock and GOLD predicted an identical binding solution for compounds **11–13**. As depicted in Figure 6, the structure of **11** fits into the Cdc25B binding cavity with the carbonyl oxygen at position 4 engaged in two hydrogen bonds with the Arg544 side chain. A salt bridge between the negatively charged carboxylate group at position 3 and the positively charged side chain of Arg482 was also observed. Moreover, the thiophenyl group at position 8 adapts itself into the Cdc25B catalytic site, establishing a T-shaped charge-transfer interaction with Phe475 through its aromatic ring. This is consistent with our other results.

Both the phenolic OH and the methoxy group of **12** are involved in hydrogen bonds with the Arg482 side chain, while the protonated amino group of the *p*-nitrophenyl alkyl chain of **12** forms an ionic interaction with the negatively charged Glu478 side chain (Figure 7). Furthermore, the *p*-nitrophenyl ring inserts into the Cdc25B catalytic site, where the nitro group hydrogen bonds with the catalytic backbone NHs of Phe475, Ser477 and Glu478.

For compound **13**, AutoDock found a well-defined cluster ($f_{\text{occ}}=19/50$, $\Delta G_{\text{bind}}=-9.48$ kcal mol⁻¹), even though this solution did not belong to the top-ranking ones. The associated binding mode, illustrated in Figure 8, is characterized by the presence of a salt bridge between the ligand's carboxylate group and the Arg544 guanidinium group, and a hydrogen-bond interaction between the furan oxygen atom and the Thr547 side chain. Moreover, the benzyl moiety in the carboxylate group's α -position is placed in Cdc25B's catalytic domain, thus making a T-shaped interaction with the Phe475 side chain.

Discussion

The development of novel and potent Cdc25B phosphatase inhibitors has always been hampered by the lack of detailed structural information about the interaction between Cdc25s and their ligands. It is still unclear how ligands actually bind within the enzyme's active site and whether general principles of binding exist that could be explored for the design of more potent compounds. Therefore, we report herein a docking study of several structurally representative Cdc25B inhibitors in order to provide a possible explanation for their inhibition mechanism. Moreover, this study should help to clarify the peculiar characteristics required for the inhibitory activity displayed by the examined compounds. With this purpose, ligands **1–13** (Tables 1–4) were subjected to docking calculations in the 3D crystal structure of Cdc25B.^[18] From all the available docking software, we chose AutoDock and GOLD, which both use genetic algorithms and have been reported to be particularly effective in reproducing experimental ligand binding modes.^[20,21,24] The choice of employing two different

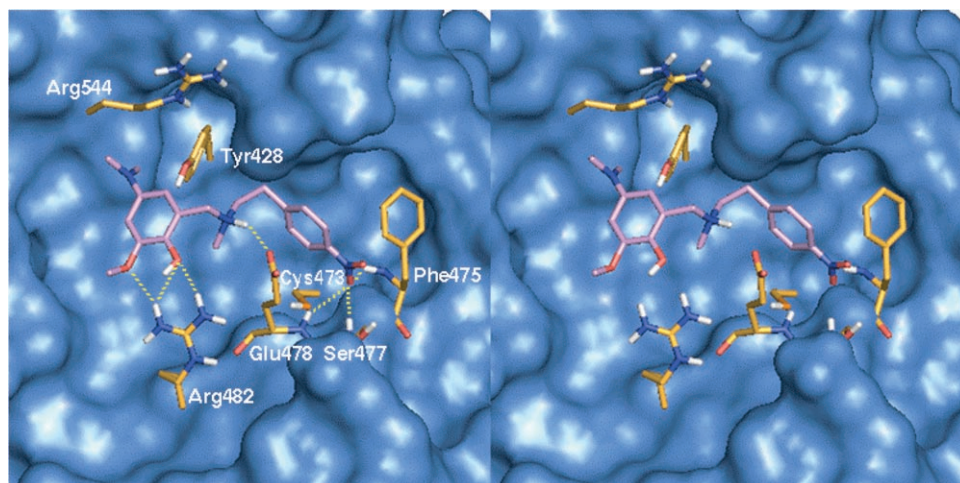


Figure 7. Stereoview of the binding mode of compound **12** in the Cdc25B binding cavity as calculated by both Autodock and GOLD.

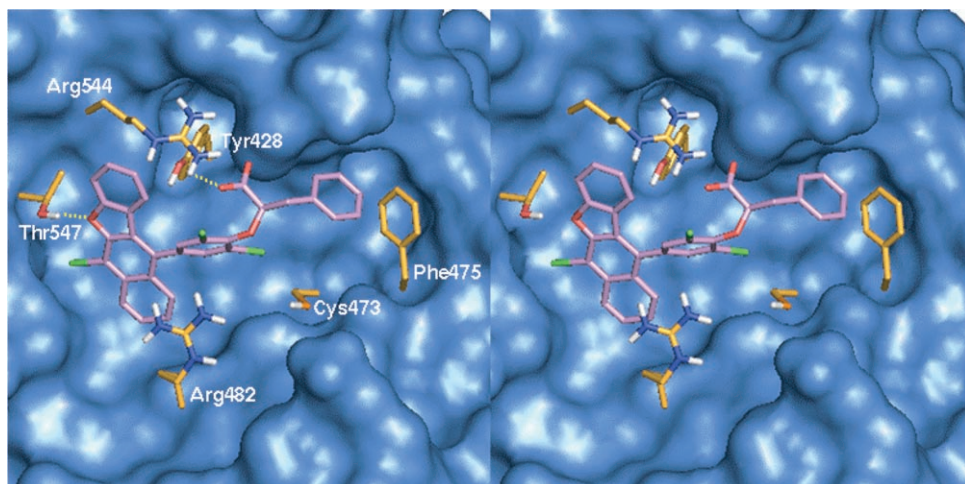


Figure 8. Stereoview of the binding mode of compound **13** in the Cdc25B binding cavity as calculated by both Autodock and GOLD.

and efficient docking protocols was dictated by the demands of achieving a mutual validation for the predicted binding positions. In fact, the inspection of a well-defined binding mode for each inhibitor of Cdc25B was complicated by the architecture of the binding-site region of Cdc25B itself, which is not a deep cleft but rather a comparatively large and shallow pocket, which allows for several reasonable and different ligand-binding poses.

Validation of the binding poses on the basis of SARs and mutagenesis data

The parallel employment of AutoDock and GOLD was supportive when inspecting the binding mode of quinolinequinones **1–4**. In fact, AutoDock was successful in predicting a single binding position for such ligands with the quinolinequinone moiety hydrogen bonding Arg482 and Arg544 through its car-

bonyl oxygens, and the pendant chain lying in the enzyme's catalytic site (Figures 1a and 2a). There are four arginine residues (Arg479, 482, 544, and 548) in the active site of the enzyme that can recognize the substrate phosphate group. Therefore, the involvement of Arg482 and Arg544 in ligand binding could explain the inhibitory activity of **1–4** against Cdc25B, in accordance with what has already been postulated by Lazo et al.^[25] Moreover, the participation of these residues in the binding of Cdc25B inhibitors was reported in a patent application by BASF, which includes the X-ray structure of a Cdc25B/inhibitor-complex.^[31] In contrast to what AutoDock predicted, the best scoring solutions of GOLD placed the quinolinequinone moiety in the Cdc25B catalytic site and the pendant chain in the region between Arg482 and Arg544. From these calculations, it could be assumed that two different binding modes are possible for compounds **1–4**, and the preference for one of them cannot be determined unambiguously (Figure 9). Interestingly, when tested for their inhibitory activity against Cdc25B, many compounds in this series displayed partial or full mixed inhibition kinetics.^[25] This might suggest that such ligands are able to inhibit the enzyme in

both a reversible and irreversible manner.

The known electrophilic properties of quinones suggest two possible interactions with the enzyme: i) the possibility of inducing a sulfhydryl arylation of a cysteine in the catalytic domain of Cdc25B or ii) an ether linkage of a serine.^[32] On the other hand, quinones can also inactivate the enzyme through redox cycling, thus oxidizing the catalytic thiolate group of Cys473. Only the latter inhibition mechanism was recently detected by Brisson and co-workers^[33] on quinone **1**, which, together with its congener JUN1111, inhibited Cdc25B in an irreversible, time-dependent manner. The observation that the *in vitro* inhibition displayed by **1** and JUN1111 was sensitive to pH, catalase, and reductants also supports an oxidative inhibition mechanism. Moreover, mass spectrometric analysis of the Cdc25B catalytic domain revealed that the catalytic Cys473 was irreversibly oxidized to a sulfonic acid, and no evidence of the addition product (**1**+Cdc25B) or an aromatization of the

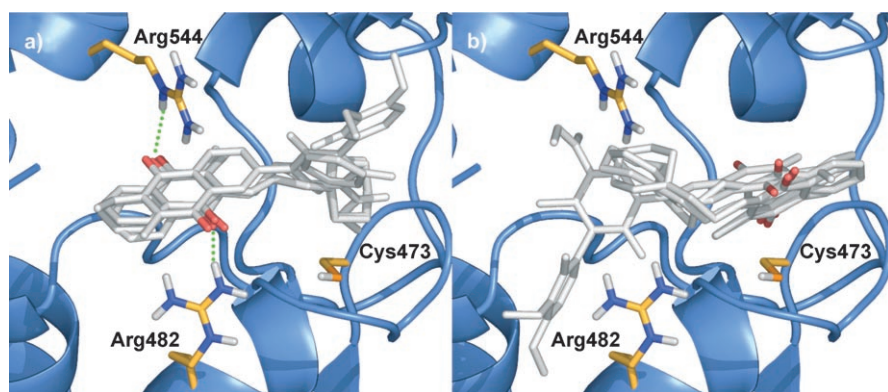


Figure 9. Alternative binding modes of quinones 1–4 superimposed into the Cdc25B active site. Ligands (white with the exception of the red quinone oxygens) and interacting key residues (orange) are represented as stick models, while the protein as a secondary structure cartoon. Hydrogen bonds are shown with dashed green lines.

product (sulfhydryl arylation) was found in this experiment.^[33] Taken together, these findings suggest that the congeneric quinones 2–4 could also have a redox inhibition mechanism. From this point of view, the capacity of 1–4 to oxidize the crucial Cys473 thiolate supports the binding pose predicted by GOLD (Figures 1b and 2b), in which the quinolinequinone moiety is in close proximity to the catalytic Cys473. Thus, it could be inferred that, when this moiety fits into the catalytic site of the enzyme, an irreversible inhibition takes place. On the other hand, the reversible inhibition displayed by 1 might be due to a reversible binding with Cdc25B or, alternatively, reversible oxidation of the enzyme's catalytic residues. Actually, it has been reported that a mild oxidation of protein phosphatases can lead to the reversible oxidation of the catalytic cysteine residue to sulfenic acid (Cys-SO⁻), which is readily reversible by cellular reductants.^[34,35] Therefore, we speculate that the reversible inhibition can occur through the formation of a reversibly oxidized adduct (this still supports the GOLD solutions) or, alternatively, through the placement of the quinolinequinone moiety in the region between Arg482 and Arg544, as suggested by the AutoDock solutions (Figures 1a and 2a).

In contrast to our results for ligands 1–4, both docking programs converged toward a single binding pose for compounds 5 and 6, in which the quinone moiety fits in the region between the Arg482 and Arg544 residues. However, neither AutoDock nor GOLD was able to detect a binding pose featuring the quinone ring in the Cdc25B catalytic site, this suggests reversible binding for 5 and 6. Interestingly, no irreversible inhibition mechanism was reported for these compounds. Two binding positions were found for inhibitors 7 and 8 in which the quinone ring fits either in the region between Arg482 and Arg544 (Figure 4a) or in the Cdc25B catalytic site (Figure 4b). Several site-directed mutagenesis data were reported for this set of compounds.^[26] In particular, the mutants Glu474Gln, Phe475Ala, and Arg482Leu, and the truncated form of Cdc25B, which lacks the last 17 residues, showed significantly altered activity toward 7, while mutation of Arg544 to Leu did not affect the activity of this compound. These data indicate that Arg544 might not interact with 7 and 8. In this respect, only

the solution in which the quinone moiety fits into the Cdc25B catalytic site seems to be plausible. Remarkably, this binding pose places the R² substituent in close proximity to the C-terminal portion of the enzyme, as is further corroborated by the results obtained when testing an analogue of 7 that is unsubstituted at R² on the above-reported Cdc25B mutants.^[26] In fact, the truncation of the last 17 amino acids of the C-terminal portion of the enzyme caused a loss in activity of 7, while it did not have any effect on the activity of the R²-unsubstituted analogue.

Taken together, these considerations strongly support the binding pose in which the quinone ring fits into the catalytic site. It could be argued that the insertion of this moiety in the catalytic loop might allow reactions with the essential Cys473 thiolate or redox reactions, thus irreversibly inactivating the enzyme. However, the reactivities of the indolyldihydroxyquinones 7 and 8^[26] proved to be dissimilar to those reported for the quinones 1–4.^[32,36] In fact, as suggested by Finley et al.,^[37] indolyldihydroxyquinones are quite electron rich, with two electron-donating hydroxyl groups and an electron-donating indole substituent, which make them much less likely to accept nucleophiles. Moreover, when the redox properties of the indolyldihydroxyquinones were investigated, it was shown that they do not sustain redox cycling (cyclic voltammetry) in aqueous DMF.^[38] These findings might explain why 7 and 8 are not capable of irreversibly inhibiting the enzyme, whereas they are able to reversibly and competitively inhibit it, even though the quinone ring may be situated in the Cdc25B catalytic site.

Docking of 9 and 10 demonstrated that they are less able to establish strong polar and electrostatic interactions with the enzyme, compared to the quinones reported so far. This might explain the high ΔG_{bind} values calculated by AutoDock and the poor scores found by GOLD, which indicate poor inhibitory activity, consistent with the high experimental IC₅₀ values. Similarly to quinones 1–4, docking of 11 into the Cdc25B binding site positioned the naphthyridinone ring in the region between Arg482 and Arg544, where the negatively charged carboxylate group is salt-bridged with the positively charged side chain of Arg482. The importance of this interaction is supported by the SAR data, since the esterification of the carboxylate group resulted in a less active compound (IC₅₀ = 120 μM).^[28]

Conclusions

The goal of this study was to explore the possible binding modes of several Cdc25B inhibitors that have high molecular diversity and inhibitory potencies ranging from micromolar to nanomolar values. The relatively open architecture of the enzyme's binding site, together with the absence of a reported

cocrystal structure of the protein with an inhibitor made this task extremely challenging. Therefore, two different automatic docking programs, AutoDock and GOLD, were employed to achieve a mutual validation of the obtained results.

According to our docking study, polar and electrostatic interactions play a crucial role in the binding of all examined ligands with the enzyme. The strength and stability of such interactions (hydrogen bonds and salt bridges) determine the inhibitory activity of these compounds toward Cdc25B. More precisely, docking experiments revealed that the quinone ring of compounds 1–6 adapts itself between Arg482 and Arg544, with the two oxygens acting as hydrogen-bond-acceptor groups. Therefore, it seems clear that the quinone moiety is crucial for Cdc25 inhibition. Moreover, the pendant chain on the quinone ring points toward the Cdc25B catalytic site, thus impeding the interaction with the protein substrate. These findings offer an explanation for the competitive inhibition reported.

The use of two different docking softwares allowed us to predict a second plausible binding position for compounds 1–4, in which the quinone ring fits into the catalytic site of Cdc25B, in close proximity to the crucial Cys473 thiolate, so as to permit its oxidation, as suggested by Brisson et al.^[33] Taken together, such results might explain the partial or full mixed inhibition kinetics displayed by compounds 1–4. A similar binding position was also found for compounds 7 and 8, in which the hydroxyquinone ring adapts itself to the Cdc25B catalytic site. However, the different reactivities of quinones 7 and 8 compared to those of 1–4 do not support an irreversible enzyme inhibition. The importance of hydrogen bonds and electrostatic interactions between the enzyme and its inhibitors was also underscored by the lower activity of aminothiazoles 9 and 10. In fact, according to our studies, such compounds are less able to establish strong electrostatic interactions with the enzyme, especially with Arg482. Similarly, the absence of interactions with this residue appears to be the main reason for the poor activity of the naphthyridinone 11.

In summary, the present study clarifies the specific structural features responsible for the activity of a set of competitive Cdc25B inhibitors. From this point of view, the presented results might provide useful hints in guiding the rational design of new potent Cdc25B inhibitors as novel anticancer drugs. Moreover, the use of two different and efficient docking programs, such as GOLD and AutoDock, proved to be a successful approach for the definition of the binding modes when the architecture of the binding region appears to allow multiple binding poses.

Computational Methods

Molecular modeling and graphics manipulations were performed by using the SYBYL software package (Sybyl Molecular Modeling System, version 7.0, Tripos Inc., St. Louis, MO) running on a Silicon Graphics Tezro workstation equipped with four 700 MHz R16000 processors. Model building of compounds 1–13 was accomplished with the TRIPOS force field^[39] available within SYBYL. Point charges for the ligands were calculated according to the Gasteiger–Marsili

method.^[40] Energy minimizations were carried out by employing the INSIGHT II/DISCOVER program (Insight II Molecular Modeling Package and Discover 2.2000 Simulation Package, Accelrys Inc., San Diego, CA), selecting the CVFF force field.^[41]

Docking simulations: Automated docking studies were performed with two different docking genetic algorithms, AutoDock 3.05^[20,21] and GOLD 2.2.^[22–24] AutoDock combines a rapid energy evaluation through precalculated grids of affinity potentials, with a variety of search algorithms to find suitable binding positions for a ligand on a given protein. While the protein is required to be rigid, the program allows torsional flexibility in the ligand. GOLD is an automated ligand-docking program that uses a genetic algorithm to explore the full range of ligand conformational flexibility with partial flexibility of the receptor. GOLD requires a user-defined binding site. It searches for a cavity within the defined area, and considers all the solvent-accessible atoms in that area as active-site atoms. On the basis of the GOLD score, the bound conformation with the highest score was considered to be the best for each molecule. The scoring function that was implemented in GOLD consisted of hydrogen-bonding, complex energy, and ligand internal-energy terms. A population of possible docked orientations for the ligand was set up at random. Each member of the population was encoded as a “chromosome” that contained information about the mapping of ligand hydrogen-bonding atoms onto (complementary) protein hydrogen-bonding atoms, hydrophobic points on the ligand onto protein hydrophobic points, and the conformation around flexible ligand bonds and protein OH groups. A number of parameters controlled the precise operation of the genetic algorithm.

Ligand setup: The core structures of ligands 1–13 were retrieved from the Cambridge Structural Database (CSD)^[42] and modified by using the standard bond lengths and bond angles of the SYBYL fragment library. Geometric optimizations were carried out with the SYBYL/MAXIMIN2 minimizer by applying the BFGS (Broyden, Fletcher, Goldfarb and Shannon) algorithm^[43] and setting a rms gradient of the forces acting on each atom of 0.05 kcal mol⁻¹ Å as the convergence criterion. Partial atomic charges were assigned by using the Gasteiger–Marsili formalism.

Protein setup. The crystal structure of Cdc25B (PDB ID: 1QB0),^[18] recovered from Brookhaven Protein Database, was used. The structure was set up for docking as follows: polar hydrogens were added by using the BIOPOLYMERS module within the SYBYL program (residues Arg, Lys, Glu, and Asp were considered ionized, while all His were considered to be neutral by default), Kollman united-atom partial charges were assigned, and all waters were removed.

AutoDock docking: Docking of 1–13 to Cdc25B was carried out by using the empirical free-energy function and the Lamarckian genetic algorithm.^[20] A standard protocol was applied, which had an initial population of 50 randomly placed individuals, a maximum number of 1.5×10^6 energy evaluations, a mutation rate of 0.02, a crossover rate of 0.80, and an elitism value of 1. Proportional selection was used, in which the average of the worst energy was calculated over a window of the previous 10 generations. For the local search, the so-called pseudo-Solis and Wets algorithm was applied by using the default parameters.

Results differing by less than 1.5 Å in positional rmsd were clustered together and represented by the result with the most favorable free energy of binding. Selected compounds were set up for docking with the help of AutoTors,^[20,21] in order to define the torsional degrees of freedom to be considered during the docking

process. All torsion angles for each compound were considered to be flexible. Solvation parameters were added to the final protein file by using the Addsol utility of AutoDock. The grid maps representing the proteins in the actual docking process were calculated with AutoGrid. The grids (one for each atom type in the ligand, plus one for electrostatic interactions) were chosen to be sufficiently large to include not only the active site, but also significant portions of the surrounding surface. The dimensions of the grids were thus 60 Å × 60 Å × 60 Å, with a spacing of 0.375 Å between the grid points. The grid center was set to be coincident with the center of the enzyme catalytic site.

GOLD docking. The active site was defined to encompass all atoms within a sphere of 20 Å radius, whose origin was located at the center of the catalytic site. The standard Genetic Algorithm protocol was selected, and the default parameters were applied for the docking. Fifty independent docking runs were performed for each docking experiment. The best 20 solutions for each ligand were ranked according to the scores, which were calculated by the native GOLD scoring function.

Energy refinement of the Cdc25B/ligand complexes: In order to eliminate any residual geometric strain, the obtained complexes were energy minimized by using 3000 steps of steepest descent, followed by 2000 steps of conjugate gradient; this permitted only the ligand and the protein side-chain atoms to relax. The geometry optimization was carried out by employing the DISCOVER program with the CVFF force field.

Figures 1–9 were created by using PYMOL software.^[44]

Acknowledgements

This work was supported by a grant from Ministero dell'Università e della Ricerca Scientifica.

Keywords: antitumor agents · Cdc25B inhibitors · docking · drug design · molecular modeling

- [1] a) E. H. Fischer, H. Charbonneau, N. K. Tonks, *Science* **1991**, *253*, 401–406; b) R. L. Stone, J. E. Dixon, *J. Biol. Chem.* **1994**, *269*, 31323–31326; c) H. Sun, N. K. Tonks, *Trends Biochem. Sci.* **1994**, *19*, 480–485, and references therein.
- [2] J. M. Denu, J. A. Stuckey, M. A. Saper, J. E. Dixon, *Cell* **1996**, *87*, 361–364.
- [3] E. B. Fauman, C. Yuvaniyama, H. L. Schubert, J. A. Stuckey, M. A. Saper, *J. Biol. Chem.* **1996**, *271*, 18780–18788.
- [4] D. Barford, *Trends Biochem. Sci.* **1996**, *21*, 407–412.
- [5] D. Barford, A. K. Das, M.-P. Eglhoff, *Annu. Rev. Biophys. Biomol. Struct.* **1998**, *27*, 133–164.
- [6] Z. Y. Zhang, *Crit. Rev. Biochem. Mol. Biol.* **1998**, *33*, 1–52.
- [7] I. Nilsson, I. Hoffmann, *Prog. Cell Cycle Res.* **2000**, *4*, 107–114.
- [8] K. Galaktionov, A. K. Lee, J. Eckstein, G. Draetta, J. Meckler, M. Loda, D. Beach, *Science* **1995**, *269*, 1575–1577.
- [9] K. Galaktionov, X. Chen, D. Beach, *Nature* **1996**, *382*, 511–517.
- [10] M. Giulia Cangini, B. Cukor, P. Soung, S. Signoretti, J. G. Moreira, M. Rana-shinge, B. Cady, M. Pagano, M. Loda, *J. Clin. Invest.* **2000**, *106*, 753–776.
- [11] S. Jinno, J. Suto, A. Nagata, M. Igarashi, Y. Kanaoka, H. Nojima, H. Okayama, *EMBO J.* **1994**, *13*, 1549–1556.
- [12] M. Molinari, C. Mercurilo, J. Dominguez, F. Goubin, G. F. Draetta, *EMBO Rep.* **2000**, *1*, 71–79.
- [13] N. Mailand, J. Falck, C. Lukas, R. G. Syljuasen, M. Welcker, J. Lukas, *Science* **2000**, *288*, 1425–1429.
- [14] a) D. Gasparotto, R. Maestro, S. Piccinin, T. Vukosavljevic, L. Barzan, S. Sulfaro, M. Baiocchi, *Cancer Res.* **1997**, *57*, 2366–2368; b) Y. Kudo, W. Yasui, T. Ue, S. Yamamoto, H. Yokozaki, H. Nikai, E. Tahara, *Jpn. J. Cancer Res.* **1997**, *88*, 9947–9952; c) W. Wu, Y. H. Fan, B. L. Kemp, G. Walsh, L. Mao, *Cancer Res.* **1998**, *58*, 4082–4085; d) D. Dixon, T. Moyana, M. J. King, *Exp. Cell Res.* **1998**, *240*, 236–243; e) S. Hernandez, L. Hernandez, S. Bea, M. Cazorla, P. L. Fernandez, A. Nadal, J. Muntane, C. Mallofre, E. Monterrat, A. Cardesa, E. Campo, *Cancer Res.* **1998**, *58*, 1762–1767.
- [15] K. Galaktionov, C. Jessup, D. Beach, *Genes Dev.* **1995**, *9*, 1046–1058.
- [16] J. W. Eckstein, *Invest. New Drugs* **2000**, *18*, 149–156.
- [17] E. B. Fauman, J. P. Cogswell, B. Lovejoy, W. J. Rocque, W. Holmes, V. G. Montana, H. Piwnica-Worms, M. J. Rink, M. A. Saper, *Cell* **1998**, *93*, 617–625.
- [18] R. A. Reynolds, A. W. Yem, C. L. Wolfe, J. Deibel, C. G. Chidester, K. D. Watenpaugh, *J. Mol. Biol.* **1999**, *293*, 559–568.
- [19] a) J. Yuvaniyama, J. M. Denu, J. E. Dixon, M. A. Saper, *Science* **1996**, *272*, 1328–1331; b) J. A. Stuckey, H. L. Schubert, E. B. Fauman, Z. Y. Zhang, J. E. Dixon, M. A. Saper, *Nature* **1994**, *370*, 571–575.
- [20] G. M. Morris, D. S. Goodsell, R. S. Halliday, R. Huey, W. E. Hart, R. K. Belew, A. J. Olson, *J. Comput. Chem.* **1998**, *19*, 1639–1662.
- [21] D. S. Goodsell, G. M. Morris, A. J. Olson, *J. Mol. Recognit.* **1996**, *9*, 1–5.
- [22] G. Jones, P. Willett, R. C. Glen, *J. Mol. Biol.* **1995**, *245*, 43–53.
- [23] G. Jones, P. Willett, R. C. Glen, A. R. Leach, R. Taylor, *J. Mol. Biol.* **1997**, *267*, 727–748.
- [24] R. Wang, Y. Lu, S. Wang, *J. Med. Chem.* **2003**, *46*, 2287–2303.
- [25] J. S. Lazo, K. Nemoto, K. E. Pestell, K. Cooley, E. C. Southwick, D. A. Mitchell, W. Furey, R. Gussio, D. W. Zaharevitz, B. Joo, P. Wipf, *Mol. Pharmacol.* **2002**, *61*, 720–728.
- [26] J. Sohn, B. Kiburz, Z. Li, L. Deng, A. Safi, M. C. Pirrung, J. Rudolph, *J. Med. Chem.* **2003**, *46*, 2580–2588.
- [27] P. Wipf, D. C. Aslan, E. C. Southwick, J. S. Lazo, *Bioorg. Med. Chem. Lett.* **2001**, *11*, 313–317.
- [28] H. I. El-Subbagh, A. H. Abadi, I. E. Al-Khawad, K. A. Al-Rashood, *Arch. Pharm.* **1999**, *332*, 19–24.
- [29] M. C. Brezak, M. Quaranta, O. Mondésert, M. O. Galcera, O. Laverigne, F. Alby, M. Cazales, V. Baldin, C. Thuriou, J. Harnett, C. Lanco, P. G. Kasprzyk, G. P. Prevost, B. A. Ducommun, *Cancer Res.* **2004**, *64*, 3320–3325.
- [30] H. G. Cheon, S. M. Kim, S. D. Yang, J. D. Ha, J. K. Choi, *Eur. J. Pharmacol.* **2004**, *485*, 333–339.
- [31] N. R. Taylor, D. Borhani, D. Epstein, J. Rudolph, K. Ritter, T. Fujimori, S. Robinson, J. Eckstein, A. Haupt, N. Walker, R. Dixon, D. Choquette, J. Blanchard, A. Kluge, K. Pal, N. Bockovich, J. Come, M. Hediger (BASF AG, Germany; GPC Biotech Inc., USA) WO 01/16300A2, **2001**.
- [32] T. W. Gant, D. N. R. Rao, R. P. Mason, G. M. Cohen, *Chem.-Biol. Interact.* **1988**, *65*, 157–173.
- [33] M. Brisson, T. Nguyen, P. Wipf, B. Joo, B. W. Day, J. S. Skoko, E. M. Schreiber, C. Foster, P. Bansal, J. Lazo, *Mol. Pharmacol.* **2005**, *68*, 1810–1820.
- [34] G. Bührman, B. Parker, J. Sohn, J. Rudolph, C. Mattos, *Biochemistry* **2005**, *44*, 5307–5316.
- [35] J. Sohn, J. Rudolph, *Biochemistry* **2003**, *42*, 10060–10070.
- [36] M. Jaffar, M. A. Naylor, N. Robertson, I. J. Stratford, *Anti-Cancer Drug Des.* **1988**, *13*, 593–609.
- [37] "The Addition and Substitution Chemistry of Quinones" K. T. Finley in *The Chemistry of the Quinonoid Compounds, Part II* (Ed.: S. Patai), Wiley, London, **1974**, p. 878.
- [38] K. Liu, L. Xu, D. Szalkowski, Z. Li, V. Ding, G. Kwei, S. Huskey, D. E. Moller, J. V. Heck, B. B. Zhang, A. B. Jones, *J. Med. Chem.* **2000**, *43*, 3487–3349.
- [39] J. G. Vinter, A. Davis, M. R. Saunders, *J. Comput.-Aided Mol. Des.* **1987**, *1*, 31–55.
- [40] J. Gasteiger, M. Marsili, *Tetrahedron* **1980**, *36*, 3219–3228.
- [41] A. F. Hagler, S. Lifson, P. Dauber, *J. Am. Chem. Soc.* **1979**, *101*, 5122–5130.
- [42] F. H. Allen, S. Bellard, M. D. Brice, B. A. Cartwright, A. Doubleday, H. Higgs, T. Hummelink, B. G. Hummelink-Peters, O. Kennard, W. D. S. Motherwell, *Acta Crystallogr. Sect. B Struct. Crystallogr. Cryst. Chem.* **1979**, *35*, 2331–2339.
- [43] J. Head, M. C. Zerner, *Chem. Phys. Lett.* **1985**, *122*, 264–274.
- [44] W. L. DeLano, The PyMOL Molecular Graphics System, **2002**, <http://www.pymol.org>.

Received: November 30, 2005

Published online on April 20, 2006